INTERNATIONAL JOURNAL FOR NUMERICAL METHODS IN ENGINEERING
Int. J. Numer. Meth. Engng 2005; **62**:1789–1806
Published online 9 February 2005 in Wiley InterScience (www.interscience.wiley.com). DOI: 10.1002/nme.1247

Vibrations of skewed cantilevered triangular, trapezoidal and parallelogram Mindlin plates with considering corner stress singularities

C. S. Huang[1,*,†,§], A. W. Leissa[2,¶] and M. J. Chang[1,‖]

[1]*Department of Civil Engineering, National Chiao Tung University, 1001 Ta-Hsueh Rd., Hsinchu, Taiwan*
[2]*Department of Mechanical Engineering, Fort Collins, Colorado, U.S.A.*

SUMMARY

Based on the Mindlin shear deformation plate theory, a method is presented for determining natural frequencies of skewed cantilevered triangular, trapezoidal and parallelogram plates using the Ritz method, considering the effects of stress singularities at the clamped re-entrant corner. The admissible displacement functions include polynomials and corner functions. The admissible polynomials form a mathematically complete set and guarantee the solution convergent to the exact frequencies when sufficient terms are used. The corner functions properly account for the singularities of moments and shear forces at the re-entrant corner and accelerate the convergence of the solution. Detailed convergence studies are carried out for plates of various shapes to elucidate the positive effects of corner functions on the accuracy of the solution. The results obtained herein are compared with those obtained by other investigators to demonstrate the validity and accuracy of the solution. Copyright © 2005 John Wiley & Sons, Ltd.

KEY WORDS: vibration; skewed; cantilevered; Mindlin; plates; singularities

1. INTRODUCTION

A cantilevered skewed trapezoidal plate, as depicted in Figure 1, has been found in numerous engineering applications, including aircraft and guided missiles. A cantilevered skewed triangular plate or parallelogram plate can be treated as a special case of a trapezoidal plate. In Figure 1, $c/b = 0$ represents a skewed triangular plate while $c/b = 1$ specifies a parallelogram plate.

*Correspondence to: C. S. Huang, Department of Civil Engineering, National Chiao Tung University, 1001 Ta-Hsueh Rd., Hsinchu, Taiwan.
†E-mail: cshuang@mail.nctu.edu.tw
§Professor.
¶Adjunct Professor.
‖Graduate student.

Contract/grant sponsor: National Science Council, R.O.C.; contract/grant number: NSC92-2211-E-009-043

Received 16 January 2004
Revised 23 June 2004
Accepted 3 August 2004

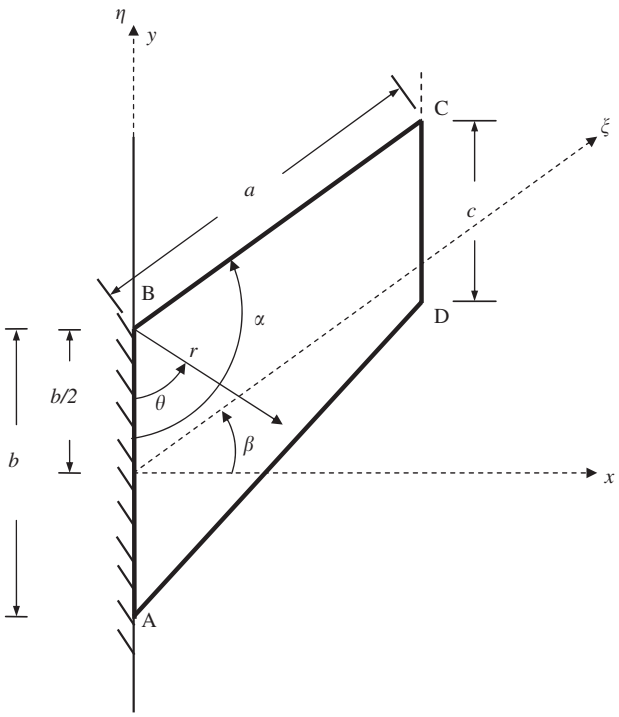

Figure 1. Geometry and co-ordinate systems of skewed cantilevered trapezoidal plate.

Because of the complexity of the geometrical shape and the boundary conditions, no exact solution is tractable for the free vibrations of such plates. Many numerical solutions, based on classical thin plate theories, have been published for such plates. Leissa [1–4] reviewed much of the earlier work in this field, while more recent work was mentioned in References [5] and [6]. Generally, one finds widespread significant disagreement in frequencies obtained among these numerous works published.

Shear deformation and rotary inertia are well known to be important to any analysis of moderately thick plates or in determining the higher vibration frequencies of thin plates. Nevertheless, rather few results have been published on the vibration frequencies of skewed triangular, trapezoidal and parallelogram plates as derived using plate theories including the effects of shear deformation and rotary inertia. McGee and Butalia [7] presented a higher-order finite element plate formulation for analysing the vibrations of skewed trapezoidal and triangular thick plates. Karunasena *et al.* [8] applied the pb-2 Rayleigh–Ritz method to elucidate the vibrations of cantilevered skewed triangular Mindlin plates.

To investigate vibrations of parallelogram plates, Kanaka Raju and Hinton [9] and Liew *et al.* [10] employed Mindlin plate theory, and used a finite element approach and pb-2 Rayleigh–Ritz method, respectively, while McGee and Leissa [11] used the Ritz method and three-dimensional elasticity theory. McGee and Butalia [12] thoroughly studied the vibrations of skew plates using nine-node Lagrangian isoparametric quadrilateral plate elements, based on three shear deformable thick plate theories.

Recently, Huang [13, 14] showed that corner stress singularities arise in Mindlin plate theory and Reddy's refined plate theory when the vertex angle of a wedge with clamped and free boundary conditions along its radial edges exceeds approximately 60°, or when the vertex angle of a corner with free–free edges is larger than 180°. As shown in References [5, 6] for cantilevered skewed thin plates, corner stress singularity behaviours have to be incorporated into numerical approaches in order to obtain accurate vibration frequencies. Nevertheless, in the aforementioned publications on cantilevered skewed triangular, trapezoidal and parallelogram Mindlin plates, the numerical approaches used have not considered stress singularities. In Reference [12], finite element convergence studies of cantilevered skewed thick plates reveal that the accuracy of the results obtained using a specified mesh size declines as the skew angle is increased. Furthermore, Karunasena *et al.* [8] admitted that their results, obtained by the pb-2 Rayleigh–Ritz method, are not accurate for cantilevered skewed triangular Mindlin plates with large skew angles because their approach did not incorporate the effects of stress singularities. Accordingly, the vibrations of cantilevered trapezoidal plates must be reexamined, considering corner stress singularities.

The aim of this work is to present an accurate numerical solution method for the free vibrations of skewed cantilevered triangular, trapezoidal and parallelogram Mindlin plates using the Ritz method and considering the corner stress singularities. The Ritz method has been widely applied to investigate the vibrations of structural components. For simplicity, polynomial functions are commonly selected as the admissible functions in the Ritz method. However, the Ritz method, when involving a large number of polynomial functions, is well known to yield easily a generalized eigenvalue problem with an ill-conditioned matrix. In this work, 'corner functions' are introduced into the admissible functions, which also include polynomial functions, to accelerate the convergence of solutions. The corner functions are established from the asymptotic solutions provided by Huang [13] for both moment and shear force singularities at a corner of a thick plate. Hence, the corner functions not only appropriately describe the singular behaviours at the clamped re-entrant corner of a skewed cantilevered plate, but also meet the clamped boundary conditions and free moment conditions around the re-entrant corner. Convergence studies are herein conducted for various skew angles to demonstrate the effects of corner functions on the accuracy of the numerical results. Accurate vibration frequencies of cantilevered trapezoidal plates with various skew angles, aspect ratios (a/b), chord ratios (c/b) and thickness ratios (h/b) are reported and compared to the published results obtained by other researchers to improve the currently available data base.

2. THEORETICAL FORMULATION

For the free vibration of a plate in Cartesian co-ordinates (x, y), the maximum strain energy $(V_{\max})$ and the maximum kinetic energy $(T_{\max})$ are (cf. Reference [8])

$$V_{\max} = \int\int_A \frac{D}{2} \left\{ \left[\psi_{x,x}^2 + \psi_{y,y}^2 + 2\upsilon\psi_{x,x}\psi_{y,y} + \frac{1-\upsilon}{2} (\psi_{x,y} + \psi_{y,x})^2 \right] + \frac{\kappa^2 G h}{2} \left[(\psi_x + w_{,x})^2 + (\psi_y + w_{,y})^2 \right] \right\} \mathrm{d}A \tag{1}$$

$$T_{\max} = \frac{\omega^2}{2}\int\int_A \left\{\rho h w^2 + \frac{\rho h^3}{12}(\psi_x^2 + \psi_y^2)\right\} \mathrm{d}A \tag{2}$$

where w is the transverse displacement of the mid-plane; ψ_x and ψ_y are the bending rotations of the mid-plane normal in the x and y directions, respectively; h is the thickness of the plate; $D = Eh^3/12(1-\upsilon^2)$ is the flexural rigidity; E is the modulus of elasticity; υ is Poisson's ratio; κ^2 is the shear correction factor; G is the shear modulus; ρ is the mass density of the plate, and ω is a free vibration frequency.

The use of skew co-ordinates (ξ, η) (Figure 1) and oblique rotations, ψ_ξ and ψ_η is usually convenient in analysing skew plates. They are related to orthogonal co-ordinates, x and y, and orthogonal rotations, ψ_x and ψ_y, by

$$\xi = x/\cos\beta, \quad \eta = y - x\tan\beta \tag{3}$$

and

$$\psi_\xi = \psi_x + \psi_y \tan\beta, \quad \psi_\eta = \psi_y/\cos\beta \tag{4}$$

where β is the skew angle of the edge BC (Figure 1). Equations (1)–(4) can be used to restate $V_{\max}$ and $T_{\max}$ in the skew co-ordinates as

$$\begin{aligned} V_{\max} = \int\int_A \Bigg\{ \frac{D}{2} \Bigg\{ & \sec^2\beta(\psi_{\xi,\xi} - \sin\beta\psi_{\xi,\eta} - \sin\beta\psi_{\eta,\xi} + \psi_{\eta,\eta})^2 \\ & - 2(1-\upsilon)\left[\psi_{\eta,\eta}\psi_{\xi,\xi} - \tfrac{1}{4}(\psi_{\xi,\eta} + \psi_{\eta,\xi})^2\right]\Bigg\} \\ & + \frac{\kappa^2 G h}{2}[(\psi_\xi - \sin\ \beta\psi_\eta + \sec\beta w_{,\xi} - \tan\beta w_{,\eta})^2 + (\cos\beta\psi_\eta + w_{,\eta})^2\Bigg\} \mathrm{d}A \end{aligned} \tag{5}$$

$$T_{\max} = \frac{\omega^2}{2}\int\int_A \left\{\rho h w^2 + \frac{\rho h^3}{12}\left[(\psi_\xi - \sin\beta\psi_\eta)^2 + (\cos\beta\psi_\eta)^2\right]\right\} \mathrm{d}A \tag{6}$$

where $\mathrm{d}A = \cos\beta\,\mathrm{d}\xi\,\mathrm{d}\eta$.

In the Ritz method, the energy functional is defined as

$$\Pi = V_{\max} - T_{\max} \tag{7}$$

$w(\xi, \eta)$, $\psi_\xi(\xi, \eta)$ and $\psi_\eta(\xi, \eta)$ in Equations (5) and (6) are approximated by finite series of admissible functions, which satisfy the geometric boundary conditions under consideration, and expressed as

$$\psi_\xi(\xi, \eta) = \Psi_{\xi\mathrm{p}}(\xi, \eta) + \Psi_{\xi\mathrm{c}}(\xi, \eta) \tag{8a}$$

$$\psi_\eta(\xi, \eta) = \Psi_{\eta\mathrm{p}}(\xi, \eta) + \Psi_{\eta\mathrm{c}}(\xi, \eta) \tag{8b}$$

$$w(\xi, \eta) = W_{\mathrm{p}}(\xi, \eta) + W_{\mathrm{c}}(\xi, \eta) \tag{8c}$$

where $\Psi_{\xi p}$, $\Psi_{\eta p}$ and W_p consist of algebraic polynomials, and $\Psi_{\xi c}$, $\Psi_{\eta c}$ and W_c consist of corner functions, which account for the singular behaviours of moments and shear forces at re-entrant corner $\angle$ABC in Figure 1. The polynomials in terms of skew co-ordinates are used; hence,

$$\Psi_{\xi p} = \sum_{i=1}^{I} \sum_{j=1}^{J} A_{ij} \xi^i \eta^{j-1} \tag{9a}$$

$$\Psi_{\eta p} = \sum_{i=1}^{I} \sum_{j=1}^{J} B_{ij} \xi^i \eta^{j-1} \tag{9b}$$

$$W_p = \sum_{i=1}^{I} \sum_{j=1}^{J} C_{ij} \xi^i \eta^{j-1} \tag{9c}$$

where A_{ij}, B_{ij} and C_{ij} are coefficients to be determined by minimizing Π. The functions given in Equation (9) satisfy the clamped edge geometric boundary conditions at $\xi = 0$. The upper limits (I, J) of the three summations in Equations (9) could all be different, but here only a single I and a single J are used, for simplification.

Although the polynomials given in Equations (9a)–(9c) constitute a mathematically complete set of admissible functions and theoretically yield accurate values of the frequencies when I and J are large enough, numerical difficulties due to ill-conditioning are very likely to occur when I and J are large. It is therefore desirable to supplement the polynomial admissible functions with the corner functions, which properly represent the singularities, to accelerate the convergence of the solution.

The sets of corner functions are

$$\Psi_{\xi c}(\xi, \eta) = \sum_{k=1}^{K} \bar{A}_k \bar{\Psi}_{\xi k}(\xi, \eta) \tag{10a}$$

$$\Psi_{\eta c}(\xi, \eta) = \sum_{k=1}^{K} \bar{B}_k \bar{\Psi}_{\eta k}(\xi, \eta) \tag{10b}$$

$$W_c(\xi, \eta) = \sum_{n=1}^{N} \bar{C}_n \bar{W}_n(\xi, \eta) \tag{10c}$$

where $\bar{A}_k$, $\bar{B}_k$ and $\bar{C}_n$ are arbitrary coefficients, and $\bar{\Psi}_{\xi k}$, $\bar{\Psi}_{\eta k}$ and $\bar{W}_n$ are established from the asymptotic solutions presented in Reference [13]. The asymptotic solutions [13] are expressed in terms of polar co-ordinates (r, θ) as shown in Figure 1. The displacement components in polar co-ordinates must transform into skew co-ordinates, yielding,

$$\bar{\Psi}_{\xi k} = (\cos\theta + \tan\beta \sin\theta)\bar{\Psi}_{\theta k} + (\sin\theta - \tan\beta \cos\theta)\bar{\Psi}_{rk} \tag{11a}$$

$$\bar{\Psi}_{\eta k} = (\sin\theta \bar{\Psi}_{\theta k} - \cos\theta \bar{\Psi}_{rk})/\cos\beta \tag{11b}$$

$$\bar{W}_n = r^{\bar{\lambda}_n} \sin \bar{\lambda}_n \theta \tag{11c}$$

where

$$\bar{\Psi}_{rk} = r^{\lambda_k}\{\cos(\lambda_k+1)\theta - k_1\eta_1\sin(\lambda_k+1)\theta - \cos(\lambda_k-1)\theta + \eta_1\sin(\lambda_k-1)\theta\} \tag{12a}$$

$$\bar{\Psi}_{\theta k} = r^{\lambda_k}\{-\sin(\lambda_k+1)\theta - k_1\eta_1\cos(\lambda_k+1)\theta + k_1\sin(\lambda_k-1)\theta + k_1\eta_1\cos(\lambda_k-1)\theta\} \tag{12b}$$

$$\eta_1 = -\frac{\lambda_k(1-\upsilon)\cos(\lambda_k+1)\alpha - (k_1(\lambda_k-1) - \lambda_k\upsilon - 1)\cos(\lambda_k-1)\alpha}{(k_1(\lambda_k-1) - \lambda_k\upsilon - 1)\sin(\lambda_k-1)\alpha - k_1\lambda_k(1-\upsilon)\sin(\lambda_k+1)\alpha} \tag{12c}$$

$$k_1 = -\frac{2(1-\upsilon) + (1+\upsilon)(\lambda_k+1)}{2(1-\upsilon) - (1+\upsilon)(\lambda_k-1)} \tag{12d}$$

$$r = \left\{\left(\frac{b}{2}-\eta\right)^2 + \xi^2 - 2\xi\left(\frac{b}{2}-\eta\right)\sin\beta\right\}^{1/2} \tag{12e}$$

$$\theta = \tan^{-1}\left(\frac{\xi\cos\beta}{(b/2-\eta) - \xi\sin\beta}\right) \tag{12f}$$

and α is the re-entrant angle (Figure 1). The characteristic values λ_k and $\bar{\lambda}_n$ are, respectively, the roots of the following equations:

$$\sin^2\lambda_k\alpha = \frac{4 - \lambda_k^2(1+\upsilon)^2\sin^2\alpha}{(3-\upsilon)(1+\upsilon)} \tag{13a}$$

and

$$\cos\bar{\lambda}_n\alpha = 0 \tag{13b}$$

Some of the λ_k arising from Equation (13a) may be complex numbers. In such cases, $\bar{\Psi}_{\xi k}$ and $\bar{\Psi}_{\eta k}$ in Equations (11a) and (11b) are complex, and both the real and imaginary parts are employed as independent functions in the solution. Notably, $\bar{\Psi}_{rk}$ and $\bar{\Psi}_{\theta k}$ in Equations (12a) and (12b) are obtained from the asymptotic solutions for singularities of bending moments, while $\bar{W}_n$ in Equation (11c) is taken from the asymptotic solutions for singularities of shear forces [13]. When the real part of λ_k is less than one, $\bar{\Psi}_{rk}$ and $\bar{\Psi}_{\theta k}$ cause bending moment singularities at the re-entrant corner, while $\bar{W}_n$ corresponding to $\bar{\lambda}_n$ smaller than one yields shear force singularities. The real parts of λ_k and $\bar{\lambda}_n$ must exceed zero to satisfy the regularity condition of finite displacement at the re-entrant corner.

Using the Ritz method, the free vibration problem is solved by substituting Equations (9a)–(9c) and (11a)–(11c) into Equations (5) and (6) and minimizing Π in Equation (7). Minimizing Π with respect to the undetermined coefficients A_{ij}, B_{ij}, C_{ij}, $\bar{A}_k$, $\bar{B}_k$ and $\bar{C}_n$ yields $3IJ + 2K + N$ homogeneous, linear algebraic equations in terms of the undetermined coefficients, which results in the matrix form of a generalized eigenvalue problem. The eigenvalues correspond to the non-dimensional vibration frequencies.

3. CONVERGENCE STUDIES AND COMPARISON

The frequencies obtained by the Ritz method should monotonically converge to the exact frequencies as upper bounds when a sufficient number of admissible functions are used, if the admissible functions are taken from a complete set of functions. This section addresses convergence studies which were carried out for cantilevered skewed triangular plates and parallelogram plates. All numerical results are presented in terms of the non-dimensional frequency parameter Ω defined as $\omega a^2\sqrt{\rho h/D}$. The results are for materials with a Poisson ratio (υ) of 0.3.

Tables I–VI present a convergence study of the non-dimensional frequency parameters of five skewed triangular plates ($a/b = 1$ or 0.5; $h/b = 0.001$ or 0.2; $\beta = 30$, 60 or 75°) and a skewed parallelogram thin plate ($a/b = 0.5$; $c/b = 1$; $\beta = 75°$; $h/b = 0.001$). The shear correction factors were set equal to $\frac{5}{6}$ to allow the present results to be compared with published data. The frequencies were obtained by increasing the number of polynomial terms in Equations (9a)–(9c) (e.g. $(I, J) = (4, 4), (5, 5), \ldots, (9, 9)$) and the number of corner functions in Equations (10a)–(10c) (e.g. $K = N = 0, 2, 5$ and 10 for $\beta = 30°$; $K = N = 0, 5, 10$ and 15 for $\beta \geqslant 60°$).

Table I. Convergence of frequency parameter Ω for a thin triangular plate ($a/b = 1$, $\beta = 30°$, $h/b = 0.001$).

Mode no.	K and N in Equations (10a)–(10c) (No. of corner functions)	(I, J) in Equations (9a)–(9c)						Reference [6]	Reference [8]
		(4, 4)	(5, 5)	(6, 6)	(7, 7)	(8, 8)	(9, 9)		
1	0	6.060	5.846	5.723	5.708	5.693	5.689	5.689	5.705
	2	5.861	5.700	5.688	5.687	5.686	5.686		
	5	5.698	5.687	5.686	5.686	5.685	5.685		
	10	5.687	5.686	5.685	5.685	5.685	5.685		
2	0	21.93	21.65	21.51	21.49	21.47	21.46	21.46	21.50
	2	21.56	21.48	21.46	21.46	21.45	21.45		
	5	21.47	21.46	21.45	21.45	21.45	21.45		
	10	21.46	21.45	21.45	21.45	21.44	21.45		
3	0	36.95	36.46	36.29	36.21	35.98	35.94	35.92	36.09
	2	36.97	35.98	35.93	35.92	35.91	35.91		
	5	36.05	35.93	35.92	35.91	35.91	35.90		
	10	35.92	35.92	35.91	35.90	35.90	35.90		
4	0	55.32	54.67	54.64	54.59	54.50	54.42	54.40	54.46
	2	54.83	54.49	54.42	54.41	54.40	54.39		
	5	54.57	54.41	54.40	54.39	54.39	54.38		
	10	54.41	54.40	54.39	54.38	54.38	54.38		
5	0	71.04	70.29	70.22	70.20	70.15	70.14	70.15	70.16
	2	70.58	70.24	70.20	70.13	70.13	70.13		
	5	70.38	70.15	70.13	70.13	70.13	70.12		
	10	70.14	70.13	70.12	70.12	70.12	70.11		

Table II. Convergence of frequency parameter Ω for a thin triangular plate ($a/b = 1,\ \beta = 60°,\ h/b = 0.001$).

Mode no.	K and N in Equations (10a)–(10c) (No. of corner functions)	(I, J) in Equations (9a)–(9c)						Reference [6]	Reference [8]
		(4, 4)	(5, 5)	(6, 6)	(7, 7)	(8, 8)	(9, 9)		
1	0	7.225	6.597	6.369	6.203	6.163	6.104	6.093	6.277
	5	6.443	6.331	6.184	6.065	6.065	6.064		
	10	6.305	6.107	6.064	6.064	6.064	6.064		
	15	6.075	6.064	6.064	6.064	6.064	6.063		
2	0	32.53	27.13	26.13	25.74	25.44	25.42	25.43	25.84
	5	26.95	25.82	25.70	25.40	25.39	25.39		
	10	25.80	25.55	25.39	25.39	25.39	25.39		
	15	25.42	25.39	25.39	25.39	25.38	25.38		
3	0	73.65	60.93	55.70	54.30	53.12	53.02	53.06	54.49
	5	66.34	54.61	53.25	52.91	52.91	52.91		
	10	53.66	53.10	52.91	52.91	52.91	52.90		
	15	53.06	52.91	52.91	52.90	52.90	52.90		
4	0	127.2	108.3	87.94	81.65	74.43	74.39	74.26	81.46
	5	110.4	85.96	80.25	74.24	74.24	74.23		
	10	90.35	79.21	74.24	74.24	74.23	74.23		
	15	75.91	74.24	74.23	74.23	74.23	74.22		
5	0	183.9	123.1	106.4	103.1	102.5	101.6	101.5	102.6
	5	142.4	108.6	102.5	101.4	101.4	101.4		
	10	122.3	101.9	101.4	101.4	101.4	101.3		
	15	101.5	101.4	101.3	101.3	101.3	101.3		

Tables I–VI show that the frequencies monotonically converge to the exact ones from above as the number of polynomial terms or the number of corner functions increases. The results obtained using only polynomial terms ($K = N = 0$) converge reasonably well for small skew angle ($\beta = 30°$) but not for large skew angles ($\beta = 60$ or $75°$). The convergence of the frequencies is significantly enhanced by augmenting the polynomial sets with an increasing number of corner functions, especially for a large skew angle. The improvement in the convergence of frequencies obtained by adding corner functions does not considerably change for different values of h/b, c/b or a/b. The results obtained using $I = J = 8$ and $K = N = 10$ are exact to at least three significant figures.

The corner functions accelerate the convergence of frequencies for two reasons. Firstly, the corner functions properly describe the behaviours of high bending and shear stresses in the vicinity of the re-entrant clamped corner. Secondly, each pair of $\bar{\Psi}_{\xi k}$ and $\bar{\Psi}_{\eta k}$ in Equations (10a) and (10b) also satisfy the boundary conditions of free moments along the free edge of the re-entrant corner.

Some of the published results obtained by others are also given in Tables I–VI. Based on classical thin plate theory, McGee *et al.* [6] applied the Ritz method and added thin plate

Table III. Convergence of frequency parameter Ω for a thin triangular plate ($a/b = 1,\ \beta = 75°,\ h/b = 0.001$).

Mode no.	K and N in Equations (10a)–(10c) (No. of corner functions)	(I, J) in Equations (9a)–(9c)						Reference [6]
		(4, 4)	(5, 5)	(6, 6)	(7, 7)	(8, 8)	(9, 9)	
1	0	8.251	7.835	7.677	7.272	6.721	6.651	6.437
	5	7.792	6.689	6.484	6.436	6.435	6.435	
	10	6.882	6.457	6.435	6.434	6.434	6.433	
	15	6.450	6.435	6.434	6.433	6.433	6.432	
2	0	32.56	31.13	30.37	29.47	28.84	27.92	27.75
	5	30.87	29.44	28.27	27.74	27.74	27.73	
	10	29.95	28.01	27.74	27.73	27.73	27.72	
	15	27.85	27.73	27.73	27.73	27.72	27.72	
3	0	76.20	72.32	71.22	69.86	68.28	67.69	66.85
	5	73.10	68.11	66.90	66.81	66.81	66.80	
	10	68.01	66.87	66.81	66.80	66.79	66.79	
	15	66.86	66.81	66.80	66.79	66.79	66.78	
4	0	139.2	131.6	128.5	123.2	120.4	118.3	117.9
	5	133.0	118.5	117.9	117.9	117.8	117.8	
	10	120.2	117.9	117.8	117.8	117.8	117.8	
	15	117.9	117.8	117.8	117.7	117.7	117.7	
5	0	209.8	179.3	165.5	154.1	151.0	146.4	144.3
	5	185.7	148.5	144.7	144.3	144.3	144.2	
	10	154.4	144.5	144.3	144.2	144.2	144.1	
	15	144.4	144.3	144.3	144.2	144.1	144.1	

theory corner functions to the algebraic polynomial admissible displacement functions. Based on Mindlin plate theory, Karunasena *et al.* [8] obtained the natural frequencies of skewed triangular plates by using the Ritz method and 120 admissible polynomial functions for each of w, ψ_ξ and ψ_η. Comparing the presented results with those of McGee *et al.* [6] reveals that the present converged results demonstrate the theoretical fact that the frequencies determined from Mindlin plate theory are less than those obtained from thin plate theory. However, the results of Karunasena *et al.* [8] violate this, indicating that these results are not accurate enough. Indeed, some of their frequencies are seen to be much too high for $\beta = 60°$. Karunasena *et al.* [8] acknowledged that the accuracy of their results become worse as the skew angle increases because stress singularity effects at the re-entrant corner were not considered. Notably, the present solution does not show the shear locking phenomenon that is often found in a finite element approach when the Mindlin plate theory is applied to a thin plate.

Table VII shows a convergence study for a cantilevered square thin plate. The shear correction factor was also set equal to $\frac{5}{6}$. According to the study on corner stress singularities induced by boundary conditions given in Reference [13], moment singularities begin to arise in the corner with free and clamped boundary conditions when the vertex angle exceeds 60°.

Table IV. Convergence of frequency parameter Ω for a thin triangular plate ($a/b = 0.5$, $\beta = 60°$, $h/b = 0.001$).

Mode no.	K and N in Equations (10a)–(10c) (No. of corner functions)	(I, J) in Equations (9a)–(9c)						Reference [6]	Reference [8]
		(4, 4)	(5, 5)	(6, 6)	(7, 7)	(8, 8)	(9, 9)		
1	0	8.663	7.183	6.599	6.163	5.947	5.883	5.846	6.112
	5	7.846	6.017	5.856	5.842	5.842	5.842		
	10	6.513	5.845	5.842	5.842	5.842	5.841		
	15	5.843	5.842	5.842	5.841	5.841	5.841		
2	0	30.96	25.33	23.65	23.15	23.00	22.97	22.95	23.26
	5	26.45	23.34	23.10	22.94	22.94	22.94		
	10	23.15	23.08	22.94	22.94	22.93	22.93		
	15	22.96	22.94	22.93	22.93	22.93	22.92		
3	0	58.37	45.65	42.70	40.49	40.14	40.05	39.56	42.23
	5	46.62	43.15	39.73	39.52	39.52	39.51		
	10	42.81	39.62	39.52	39.52	39.51	39.51		
	15	39.54	39.51	39.51	39.50	39.50	39.50		
4	0	108.0	81.40	67.16	64.67	63.29	63.05	63.16	63.92
	5	85.62	70.82	63.14	62.99	62.99	62.99		
	10	72.45	64.14	62.99	62.99	62.99	62.98		
	15	63.00	62.99	62.98	62.97	62.96	62.96		
5	0	120.4	97.40	74.26	70.23	67.43	66.37	66.64	73.89
	5	105.2	80.64	69.13	66.36	66.36	66.36		
	10	85.31	70.16	66.36	66.36	66.36	66.34		
	15	67.42	66.36	66.36	66.34	66.34	66.34		

Hence, since these angles are 90° at both clamped–free corners, one should add corner functions in corner A, as well as corner B (Figure 1). However, for simplicity, Table VII shows the results without any corner function for corner A. Although adding corner functions accelerates the convergence, the results obtained using only polynomial terms ($K = N = 0$) still converge reasonably well, which is consistent with the observation from Table I. But one also observes in Table VII that essentially the same accuracy is obtained when using 10 corner functions with $I = J = 4$ as no corner functions with $I = J = 9$. These two solutions result in eigenvalue determinants of order 68 and 243, respectively. Thus, adding corner functions does increase computational efficiency significantly. The results of Huang [15] and Leissa [16] were obtained using the Ritz method and based on classical thin plate theory. Huang [15] used the same approach as McGee *et al.* [6], while Leissa [16] used characteristic beam functions as admissible functions. Again, the present converged results for this thin plate show excellent agreement with the results from thin plate theory, especially for the results of Huang [15].

To further demonstrate the validity and accuracy of the present solutions, the frequency parameters Ω determined from this study were compared with those in the literature for various

Table V. Convergence of frequency parameter Ω for a thick triangular plate ($a/b = 1,\ \beta = 60°,\ h/b = 0.2$).

Mode no.	K and N in Equations (10a)–(10c) (No. of corner functions)	(I, J) in Equations (9a)–(9c)						Reference [8]
		(4, 4)	(5, 5)	(6, 6)	(7, 7)	(8, 8)	(9, 9)	
1	0	6.314	5.747	5.624	5.500	5.483	5.424	5.517
	5	5.622	5.534	5.458	5.410	5.410	5.409	
	10	5.509	5.449	5.409	5.409	5.409	5.408	
	15	5.432	5.409	5.409	5.408	5.408	5.408	
2	0	25.16	21.26	20.49	20.14	19.95	19.94	20.32
	5	20.98	20.42	20.00	19.93	19.93	19.92	
	10	20.29	20.20	19.93	19.93	19.92	19.92	
	15	19.99	19.93	19.92	19.92	19.92	19.91	
3	0	40.79	29.38	25.27	24.49	23.33	23.22	23.65
	5	27.39	24.64	23.98	23.20	23.19	23.19	
	10	24.56	23.41	23.19	23.19	23.19	23.19	
	15	23.28	23.19	23.19	23.19	23.18	23.18	
4	0	87.98	66.92	46.68	40.92	34.89	34.80	35.43
	5	69.74	44.60	38.92	34.75	34.75	34.75	
	10	41.03	38.01	34.75	34.75	34.75	34.74	
	15	35.66	34.75	34.74	34.74	34.74	34.73	
5	0	101.7	76.13	47.29	43.74	42.16	41.74	41.90
	5	80.46	46.95	42.45	41.27	41.27	41.27	
	10	47.37	41.75	41.27	41.27	41.26	41.26	
	15	41.66	41.27	41.26	41.26	41.25	41.25	

shapes of plates. In obtaining all of the following numerical results, $I = J = 8$ and $K = N = 2$ in Equations (9) and (10) were used for plates with $\beta \leqslant 30°$; $I = J = 8$ and $K = N = 10$ were used for plates with $\beta > 30°$. The corner functions were added to corner B only. Based on the preceding convergence study, the results given here are accurate to at least three significant figures, and almost to four digits. Tables VIII–X compare the results obtained herein with the published results for skewed triangular, trapezoidal and parallelogram thick plates, respectively. Notably, the shear correction factors were set to $\frac{5}{6}$, $\pi^2/12$ and 0.823 for triangular, trapezoidal and parallelogram plates, respectively, as they were used in the cited references.

Table VIII lists Ω of triangular plates with $h/b = 0.2$ and various a/b ratios and β values; the present results agree reasonably with those of Karunasena *et al.* [8]. However, the values of Ω obtained herein are smaller than those of Karunasena *et al.* [8], meaning that they are more accurate, because the present method guarantees upper bounds for the frequencies. The differences become more significant for plates with larger β that exhibit more serious stress singularities at the clamped re-entrant corner. There is no particular trend in the differences as affected by a/b.

Table VI. Convergence of frequency parameter Ω for a thin parallelogram plate ($a/b = 0.5,\ \beta = 75°,\ h/b = 0.001$).

Mode no.	K and N in Equations (10a)–(10c) (No. of corner functions)	(I, J) in Equations (9a)–(9c)						Reference [6]
		(4, 4)	(5, 5)	(6, 6)	(7, 7)	(8, 8)	(9, 9)	
1	0	7.477	6.915	6.785	6.435	6.295	6.184	6.054
	5	6.994	6.398	6.137	5.995	5.994	5.994	
	10	6.256	6.074	5.994	5.994	5.993	5.993	
	15	6.023	5.994	5.994	5.993	5.993	5.992	
2	0	29.83	27.31	25.20	24.77	24.68	24.81	25.00
	5	28.08	24.88	24.56	24.52	24.51	24.51	
	10	24.66	24.52	24.52	24.51	24.50	24.50	
	15	24.52	24.51	24.51	24.50	24.50	24.49	
3	0	50.04	49.87	48.68	47.85	47.34	47.25	47.21
	5	49.94	47.15	46.95	46.94	46.93	46.93	
	10	47.26	46.94	46.94	46.93	46.93	46.92	
	15	46.94	46.93	46.93	46.92	46.92	46.92	
4	0	75.35	62.53	59.49	58.37	57.52	57.42	57.86
	5	64.74	59.11	57.86	57.29	57.29	57.28	
	10	58.27	57.67	57.29	57.28	57.28	57.28	
	15	57.57	57.28	57.28	57.28	57.27	57.27	
5	0	102.0	84.95	71.36	69.48	68.92	68.59	69.05
	5	85.25	78.42	69.21	68.59	68.58	68.57	
	10	77.89	69.01	68.58	68.57	68.57	68.56	
	15	68.75	68.58	68.57	68.57	68.56	68.55	

The results of McGee and Butalia [7, 12] in Tables VIII–X were obtained using higher-order shear deformable plate theory and the finite element approach. No shear correction factor is involved. These results were obtained using 64 Lagrangian isoparametric plate elements with a total of 2448 degrees of freedom, whereas the present method used, at most, 222 degrees of freedom. The convergence studies in Reference [7] indicate that these results may converge to only two significant figures. Generally reasonably good agreement is observed between the present results and those of McGee and Butalia [7, 12], except in the cases of plates with $\beta = 75°$. McGee and Butalia [7] must have mistyped the results for $a/b = 1,\ c/b = 0.5$ and $\beta = 45°$ given in Table IX because they are exactly the same as those for $\beta = 30°$. Notably, McGee and Butalia [7] conceded that the stress singularity at the re-entrant corner should be incorporated into their finite element modeling of highly skewed plates, when they found that their results for thin plates exceeded those obtained by applying thin plate theory [6] using the Ritz method.

Table X presents Ω values of parallelogram plates with various h/b ratios and β values; the present results agree closely with those of Liew *et al.* [10], who also used the Mindlin plate theory. Nevertheless, the present results are all lower than those of Liew *et al.* [10], indicating that the present work provides better upper bounds of the exact solutions.

Table VII. Convergence of frequency parameter Ω for a thin square plate ($\beta = 0°$, $h/b = 0.001$).

Mode no.	K and N in Equations (10a)–(10c) (No. of corner functions)	(I, J) in Equations (9a)–(9c)						Reference [15]	Reference [16]
		(4, 4)	(5, 5)	(6, 6)	(7, 7)	(8, 8)	(9, 9)		
1	0	3.494	3.478	3.475	3.473	3.472	3.471	3.472	3.492
	2	3.479	3.473	3.472	3.471	3.471	3.471		
	5	3.472	3.472	3.471	3.471	3.470	3.470		
	10	3.471	3.471	3.471	3.470	3.470	3.470		
2	0	8.547	8.543	8.512	8.511	8.511	8.510	8.509	8.525
	2	8.544	8.512	8.511	8.510	8.509	8.509		
	5	8.511	8.511	8.510	8.509	8.509	8.508		
	10	8.510	8.509	8.509	8.508	8.508	8.508		
3	0	21.56	21.43	21.31	21.30	21.29	21.28	21.29	21.43
	2	21.51	21.32	21.29	21.28	21.28	21.28		
	5	21.30	21.29	21.28	21.28	21.28	21.28		
	10	21.29	21.28	21.28	21.28	21.27	21.27		
4	0	31.41	27.52	27.46	27.20	27.19	27.18	27.20	27.33
	2	27.82	27.48	27.19	27.19	27.18	27.18		
	5	27.26	27.19	27.18	27.18	27.18	27.17		
	10	27.19	27.18	27.18	27.17	27.17	27.17		
5	0	31.90	31.33	30.98	30.98	30.97	30.95	30.97	31.11
	2	31.55	30.97	30.97	30.96	30.95	30.95		
	5	30.97	30.96	30.96	30.95	30.94	30.94		
	10	30.96	30.95	30.95	30.94	30.94	30.94		

Table VIII. Comparison of frequency parameters Ω for triangular thick plates ($h/b = 0.2$).

a/b	β (deg)	Mode number			
		1	2	3	4
0.5	0	4.535 [4.540] ⟨4.542⟩	9.783 [9.801] ⟨9.873⟩	14.93 [14.98] ⟨15.03⟩	16.94 [16.99] ⟨/⟩
	15	4.273 [4.283] ⟨4.284⟩	9.452 [9.470] ⟨9.531⟩	14.40 [14.44] ⟨14.43⟩	16.24 [16.29] ⟨/⟩
	30	4.233 [4.239] ⟨4.239⟩	9.762 [9.783] ⟨9.831⟩	14.04 [14.06] ⟨13.95⟩	16.42 [16.49] ⟨16.62⟩
	45	4.335 [4.338] ⟨4.334⟩	10.58 [10.62] ⟨10.59⟩	13.41 [13.48] ⟨13.33⟩	17.46 [17.48] ⟨/⟩

Table VIII. *Continued.*

		Mode number			
a/b	β (deg)	1	2	3	4
1.0	60	4.553 [4.565] ⟨4.534⟩	9.626 [9.699] ⟨9.633⟩	13.76 [13.82] ⟨13.83⟩	15.92 [16.01] ⟨/⟩
	75	4.915 [5.031] ⟨4.925⟩	5.454 [5.567] ⟨6.264⟩	9.471 [9.672] ⟨15.37⟩	15.53 [15.64] ⟨/⟩
	0	5.740 [5.744] ⟨5.730⟩	18.74 [18.75] ⟨18.76⟩	23.75 [23.77] ⟨23.79⟩	38.82 [38.85] ⟨/⟩
	15	5.366 [5.369] ⟨5.356⟩	17.47 [17.48] ⟨17.47⟩	23.54 [23.55] ⟨23.57⟩	35.79 [35.81] ⟨/⟩
	30	5.210 [5.261] ⟨5.246⟩	17.32 [17.49] ⟨17.46⟩	23.65 [23.88] ⟨23.87⟩	34.85 [35.19] ⟨/⟩
	45	5.225 [5.330] ⟨5.306⟩	18.24 [18.60] ⟨18.57⟩	24.09 [24.57] ⟨24.49⟩	35.56 [36.26] ⟨/⟩
	60	5.409 [5.517] ⟨5.479⟩	19.92 [20.32] ⟨20.21⟩	23.19 [23.65] ⟨23.55⟩	34.75 [35.43] ⟨/⟩
	75	5.728 [5.912] ⟨5.806⟩	13.52 [14.76] ⟨15.77⟩	21.42 [22.37] ⟨21.85⟩	21.59 [22.45] ⟨/⟩
2.0	0	6.435 [6.475] ⟨6.447⟩	26.28 [26.45] ⟨26.29⟩	39.33 [39.48] ⟨39.53⟩	60.22 [60.40] ⟨/⟩
	15	6.066 [6.080] ⟨6.074⟩	24.52 [24.67] ⟨24.53⟩	39.50 [39.68] ⟨39.69⟩	56.69 [56.89] ⟨/⟩
	30	5.932 [5.961] ⟨5.939⟩	23.89 [24.32] ⟨23.90⟩	41.34 [45.44] ⟨41.51⟩	55.84 [56.61] ⟨/⟩
	45	5.948 [5.961] ⟨5.959⟩	24.18 [24.32] ⟨24.15⟩	45.34 [45.44] ⟨45.40⟩	56.57 [56.61] ⟨/⟩
	60	6.077 [6.119] ⟨6.081⟩	24.99 [25.15] ⟨24.95⟩	49.77 [49.94] ⟨49.99⟩	57.60 [57.64] ⟨/⟩
	75	6.257 [6.396] ⟨6.327⟩	26.38 [26.57] ⟨26.12⟩	35.83 [36.24] ⟨38.28⟩	50.51 [50.53] ⟨/⟩

Note: [ ] denotes values from Karunasena *et al.* [8], ⟨ ⟩ denotes values from McGee and Butalia [7], / denotes no data available.

Table IX. Comparison of frequency parameters Ω for trapezoidal thick plates ($h/b = 0.2$).

			Mode number			
a/b	c/b	β (deg)	1	2	3	4
0.5	0.25	15	3.508 ⟨3.521⟩	7.602 ⟨7.674⟩	12.71 ⟨12.86⟩	14.43 ⟨/⟩
		30	3.551 ⟨3.565⟩	7.882 ⟨7.947⟩	12.97 ⟨13.06⟩	14.52 ⟨14.65⟩
		45	3.724 ⟨3.747⟩	8.823 ⟨8.897⟩	13.25 ⟨13.27⟩	15.77 ⟨/⟩
		60	4.017 ⟨4.026⟩	10.03 ⟨10.05⟩	13.26 ⟨13.29⟩	18.40 ⟨/⟩
		75	4.448 ⟨4.455⟩	7.244 ⟨7.633⟩	12.33 ⟨14.63⟩	15.05 ⟨/⟩
	0.5	15	3.314 ⟨3.330⟩	6.087 ⟨6.147⟩	11.36 ⟨11.40⟩	12.00 ⟨12.00⟩
		30	3.461 ⟨3.472⟩	6.396 ⟨6.451⟩	11.82 ⟨11.90⟩	12.34 ⟨12.47⟩
		45	3.736 ⟨3.759⟩	7.407 ⟨7.410⟩	12.41 ⟨12.53⟩	13.49 ⟨13.52⟩
		60	4.126 ⟨4.135⟩	9.701 ⟨9.764⟩	12.92 ⟨12.88⟩	15.71 ⟨/⟩
		75	4.674 ⟨4.653⟩	7.780 ⟨8.139⟩	12.85 ⟨13.93⟩	13.54 ⟨/⟩
1.0	0.25	15	4.168 ⟨4.170⟩	14.26 ⟨14.32⟩	19.42 ⟨19.52⟩	30.91 ⟨/⟩
		30	4.152 ⟨4.153⟩	14.43 ⟨14.49⟩	20.11 ⟨20.22⟩	30.43 ⟨/⟩
		45	4.275 ⟨4.278⟩	15.73 ⟨15.80⟩	21.17 ⟨21.27⟩	32.31 ⟨/⟩
		60	4.475 ⟨4.494⟩	17.99 ⟨18.08⟩	22.16 ⟨22.18⟩	36.72 ⟨/⟩
		75	4.803 ⟨4.817⟩	17.90 ⟨18.19⟩	20.43 ⟨20.54⟩	34.60 ⟨/⟩
	0.5	15	3.772 ⟨3.774⟩	11.40 ⟨11.44⟩	18.42 ⟨18.53⟩	27.55 ⟨/⟩
		30	3.858 ⟨3.864⟩	11.76 ⟨11.81⟩	19.39 ⟨19.52⟩	27.16 ⟨/⟩
		45	4.078 ⟨3.864⟩	13.17 ⟨11.81⟩	20.68 ⟨19.52⟩	29.11 ⟨/⟩
		60	4.243 ⟨4.444⟩	16.06 ⟨16.25⟩	22.31 ⟨22.50⟩	34.60 ⟨/⟩
		75	4.718 ⟨4.887⟩	19.21 ⟨19.61⟩	21.59 ⟨21.68⟩	35.56 ⟨/⟩

Note: ⟨ ⟩ denotes values from McGee and Butalia [7], / denotes no data available.

Table X. Comparison of frequency parameters Ω for parallelogram plates ($a/b = 1$).

h/b	β (deg)	Mode number 1	2	3	4
0.1	0	3.427 [3.431] ⟨3.431⟩	8.052 [8.058] ⟨8.064⟩	20.07 [20.08] ⟨20.10⟩	25.48 [25.49] ⟨25.52⟩
	15	3.523 [3.536] ⟨3.537⟩	8.203 [8.228] ⟨8.235⟩	20.73 [20.85] ⟨20.88⟩	24.62 [24.65] ⟨24.68⟩
	30	3.856 [3.858] ⟨3.863⟩	8.862 [8.870] ⟨8.878⟩	23.23 [23.24] ⟨23.29⟩	24.21 [24.27] ⟨24.30⟩
	45	4.385 [4.387] ⟨4.401⟩	10.52 [10.54] ⟨10.55⟩	24.72 [24.77] ⟨24.82⟩	28.24 [28.26] ⟨28.32⟩
	60	4.956 [5.049] ⟨5.008⟩	14.90 [14.90] ⟨14.96⟩	26.39 [27.08] ⟨27.11⟩	38.25 [38.33] ⟨38.41⟩
0.2	0	3.335 [3.338] ⟨3.342⟩	7.333 [7.340] ⟨7.367⟩	17.53 [17.55] ⟨17.69⟩	22.42 [22.44] ⟨22.57⟩
	15	3.430 [3.434] ⟨3.439⟩	7.482 [7.489] ⟨7.516⟩	18.04 [18.06] ⟨18.18⟩	21.58 [21.60] ⟨21.74⟩
	30	3.715 [3.719] ⟨3.729⟩	8.047 [8.055] ⟨8.086⟩	19.50 [19.51] ⟨19.68⟩	21.32 [21.35] ⟨21.48⟩
	45	4.163 [4.171] ⟨4.194⟩	9.505 [9.524] ⟨9.572⟩	20.74 [20.78] ⟨21.02⟩	23.51 [23.56] ⟨/⟩
	60	4.709 [4.719] ⟨4.771⟩	13.17 [13.20] ⟨13.32⟩	22.05 [22.10] ⟨22.50⟩	28.97 [29.03] ⟨/⟩

Note: [ ] denotes values from Liew *et al.* [10], ⟨ ⟩ denotes values from McGee and Butalia [12], / denotes no data available.

Notably, Liew *et al.* [10] applied the Ritz method with admissible polynomial functions, involving 360 degrees of freedom, while the present solutions involve 198 and 222 degrees of freedom for plates with $\beta \leqslant 30^\circ$ and $\beta > 30^\circ$, respectively.

4. CONCLUDING REMARKS

This paper has demonstrated a novel Ritz procedure to determine accurately the natural frequencies of skewed cantilevered triangular, trapezoidal and parallelogram plates based on Mindlin plate theory. The proposed procedure incorporates a mathematically complete set of admissible

polynomials in conjunction with admissible corner functions that not only properly describe the singular behaviours of moments and shear forces at the re-entrant clamped corner, but also satisfy the free moment conditions along the free edge of the re-entrant corner.

The effects of adding corner functions to the admissible set of polynomials in the Ritz method on the determination of the frequencies of a plate were investigated through convergence studies for various plates with different shapes. It was shown there that use of corner functions accelerates the convergence of the solutions significantly, thereby permitting one to obtain accurate frequencies from smaller eigenvalue determinants, and reducing numerical ill-conditioning.

The highly accurate results obtained from the present solution were demonstrated through comparison with previously published data for cantilevered triangular, trapezoidal and parallelogram plates. Significant improvement (closer upper bounds) was seen especially for the thick plates with a large skewed angle ($\beta \geqslant 45°$).

The procedure demonstrated in this work can be easily modified to analyse other shapes of Mindlin plates that involve stress singularities caused by boundary conditions at a corner. Besides the clamped–free corner dealt with here, one can also apply this method to other types of sharp corners such as, for example, the free–free edges interesting at a notch or crack. Moreover, although this procedure was demonstrated here only for free vibrations, it could also be applied effectively to other plate problems, such as static loading, buckling or dynamic response.

ACKNOWLEDGEMENTS

This work was supported by the National Science Council, R.O.C. through research Grant No. NSC92-2211-E-009-043. The support is gratefully acknowledged.

REFERENCES

1. Leissa AW. *Vibration of Plates*, *NASA SP-160*. U.S. Government Printing Office, 1969 (reprinted by The Acoustical Society of America, 1993).
2. Leissa AW. Recent research in plate vibrations, 1973–1976: classical theory. *The Shock and Vibration Digest* 1977; **9**(10):13–24.
3. Leissa AW. Plate vibration research, 1976–1980: classical theory. *The Shock and Vibration Digest* 1981; **13**(9):11–22.
4. Leissa AW. Recent studies in plate vibrations: 1981–1985. Part I: classical theory. *The Shock and Vibration Digest* 1987; **19**(2):11–18.
5. McGee OG, Leissa AW, Huang CS. Vibrations of cantilevered skewed plates with corner stress singularities. *International Journal for Numerical Methods in Engineering* 1992; **35**(2):409–424.
6. McGee OG, Leissa AW, Huang CS. Vibrations of cantilevered skewed trapezoidal and triangular plates with corner stress singularities. *International Journal of Mechanical Sciences* 1992; **34**(1):63–84.
7. McGee OG, Butalia TS. Natural vibrations of shear deformable cantilevered skew trapezoidal and triangular thick plates. *Computers and Structures* 1992; **45**(5/6):1033–1059.
8. Karunasena W, Kitipornchai S, AL-Bermani FGA. Free vibration of cantilevered arbitrary triangular Mindin plates. *International Journal of Mechanical Sciences* 1996; **38**(4):431–442.
9. Kanaka Raju K, Hinton E. Natural frequencies and modes of rhombic Mindlin plates. *Earthquake Engineering and Structural Dynamics* 1980; **8**:55–62.
10. Liew KM, Xiang Y, Kitipornchai S, Wang CM. Vibration of thick skew plates based on Mindlin shear deformation plate theory. *Journal of Sound and Vibration* 1993; **168**(1):39–69.
11. McGee OG, Leissa AW. Three-dimensional free vibrations of thick skewed cantilevered plates. *Journal of Sound and Vibration* 1991; **144**:305–322.

12. McGee OG, Butalia TS. Natural vibrations of shear deformable cantilevered skew thick plates. *Journal of Sound and Vibration* 1994; **176**(3):351–376.
13. Huang CS. Stress singularities at angular corners in first-order shear deformation plate theory. *International Journal of Mechanical Sciences* 2003; **45**:1–20.
14. Huang CS. On the singularity induced by boundary conditions in a third-order thick plate theory. *Journal of Applied Mechanics* (ASME) 2002; **69**:800–810.
15. Huang CS. Singularities in plate vibration problems. *Ph.D. Dissertation*, The Ohio State University, 1991.
16. Leissa AW. The free vibration of rectangular plates. *Journal of Sound and Vibration* 1973; **31**(3):257–293.

